A Solid-State NMR and Computational Study of Sodium and Potassium Tetraphenylborates: ^{23}Na and ^{39}K NMR Signatures for Systems Containing Cation−π Interactions

Alan Wong,[†] Robert D. Whitehead,[‡] Zhehong Gan,[§] and Gang Wu*[,†]

Department of Chemistry, Queen's University, Kingston, Ontario, Canada K7L 3N6, Department of Chemistry and Chemical Engineering, Royal Military College of Canada, Kingston, Ontario, Canada K7K 7B4, and Center of Interdisciplinary Magnetic Resonance, National High Magnetic Field Laboratory, 1800 East Paul Dirac Drive, Tallahassee, Florida 32310

Received: July 19, 2004; In Final Form: September 14, 2004

Sodium and potassium tetraphenylborates were examined by solid-state ^{23}Na and ^{39}K NMR spectroscopy. Analyses of solid-state NMR spectra obtained at 4.70, 11.75, and 19.60 T yielded the following ^{23}Na and ^{39}K NMR parameters: Na[BPh_4], $|C_Q| = 1.24 \pm 0.05$ MHz, $\eta_Q = 0.0 \pm 0.1$, $\delta_{iso} = -45.6 \pm 0.5$ ppm, and $\Omega = 14 \pm 2$ ppm; K[BPh_4], $|C_Q| = 1.32 \pm 0.05$ MHz, $\eta_Q = 0.0 \pm 0.1$, and $\delta_{iso} = -92 \pm 1$ ppm. In both Na[BPh_4] and K[BPh_4], the electric field gradient and chemical shift tensors at the metal site are axially symmetric, in agreement with the crystallographic symmetry. Extensive quantum mechanical calculations were performed for Na[BPh_4] and K[BPh_4] as well as for a large number of model cation−π systems containing Na^+ and K^+ ions and common aromatic compounds. Experimental and theoretical studies confirm that a highly shielded environment at the metal cation site is a characteristic feature for cation−π interactions, making it useful as a NMR signature for identifying cation−π interactions in proteins and nucleic acids. In this study, powder X-ray diffraction spectra for Na[BPh_4] and K[BPh_4] were also reported.

Introduction

Noncovalent interactions play an essential role in molecular recognition and in biomolecular structures. In addition to conventional noncovalent interactions such as hydrogen bonding, ion pairing, and hydrophobic interactions, cation−π interactions have been recognized as an important force in biomolecular processes.[1−3] In proteins, weak cation−π interactions may occur between charged protein side chains or metal ions and aromatic amino acid residues such as phenylalanine (Phe), trptophan (Trp), tyrosine (Tyr), and histidine (His). Similar situations can also be found in nucleic acids where aromatic bases of adenine (A), guanine (G), thymine (T), uracil (U), and cytosine (C) may be involved in cation−π interactions.

For the most abundant alkali metal ions in biological systems, Na^+ and K^+, a large number of experimental and theoretical studies have been carried out for understanding the structural feature of cation−π complexes containing small organic molecules.[3] Meanwhile, fewer cases are available in the literature regarding Na^+ and K^+ ions in proteins and nucleic acids.[4,5] This is because detecting light alkali metal ions in proteins and nucleic acids by X-ray crystallography is a challenging task. Identification of Na^+ ions is particularly difficult, because a Na^+ ion has the same number of electrons as a water molecule, rendering it difficult to distinguish these two species on an electron density map. Although crystallographic methods for solving (at least partially) this ambiguity are available,[6,7] it is desirable to develop other analytical techniques that can provide complementary information about alkali metal cation binding in proteins and nucleic acids.

Our particular interest in exploring the possibility of solid-state ^{23}Na and ^{39}K NMR for probing cation−π interactions was triggered by recent proposals that some of the water molecules previously reported in protein structures may have actually been alkali metal cations. For example, Wouters[8] reported a new cation−π binding site in hen egg-white (HEW) lysozyme where a Na^+ ion is located 4 Å above the indole ring of Trp123. A similar site was identified by Wouters and Maes[9] in the crystal structure of a thermophilic *Bacillus stearothermophilus* triosephosphate isomerase mutant. Gokel and co-workers[10] also proposed that a putative water molecule in tryptophanase is an alkali metal cation, because it is located 3.7 Å above the aromatic ring of Tyr429. However, Sarkhel et al.[11] recently reported crystallographic evidence for water−nucleobase "stacking" structures in an RNA pseudokot. This type of structure is due to lone pair−π (l.p.−π) interactions between water molecules and nucleobases, for which the water−centroid distance is typically between 2.93 and 3.78 Å. It is likely that similar interactions are also operative between water and aromatic amino acid residues in proteins. Because the water−centroid distances are very similar to Na^+−centroid distances in cation−π systems, it remains unclear whether Na^+−π and water−π interactions can be unambiguously distinguished by crystallography. This further emphasizes the need for alternative techniques that may provide additional information about cation binding sites in biological macromolecules.

In principle, metal cation NMR is capable of providing direct information about cation−π interactions. However, until recently there has been very little NMR data available in this area. Beer and co-workers[12] demonstrated the use of ^{205}Tl (spin $^1/_2$) NMR

* Address correspondence to this author. E-mail: gangwu@chem.queensu.ca.
[†] Queen's University.
[‡] Royal Military College of Canada.
[§] Center of Interdisciplinary Magnetic Resonance.

10.1021/jp0468051 CCC: $27.50
Published on Web 10/30/2004

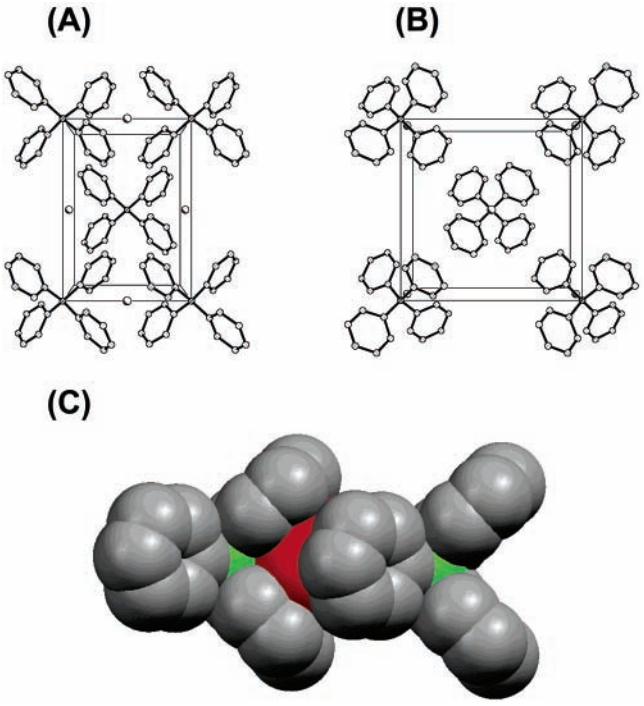

Figure 1. Unit cell for $K[BPh_4]$ viewed along the *a*-axis (A) and the *c*-axis (B). (C) Model used in quantum mechanical calculations. Hydrogen atoms are omitted for clarity. Color code: K (red), B (green), and C (gray).

in studying cation$-\pi$ interactions in solution. For alkali metal cations, several solid-state ^{7}Li and ^{23}Na NMR studies have been reported dealing with metallocene compounds.[13−16] To establish solid-state ^{23}Na and ^{39}K NMR as a tool for probing cation$-\pi$ interactions, one needs to obtain spectral signatures for such cation binding sites. Here we report a comprehensive solid-state NMR study of sodium and potassium tetraphenylborates, two earliest known compounds containing cation$-\pi$ interactions. $K[BPh_4]$ crystallizes in tetragonal form with space group $I\bar{4}2m$.[17] As shown in Figure 1, in the crystal lattice each K^+ ion is surrounded by four phenyl groups. The distance between the K^+ ion and the center of the phenyl ring is 3.343 Å. According to powder X-ray diffraction data given in the International Centre for Diffraction Data (ICDD) database,[18] $Na[BPh_4]$ is isostructural to $K[BPh_4]$ with a slightly shorter cation−centroid distance. To supplement our experimental solid-state NMR data, we also perform quantum mechanical calculations on both electric field gradient (EFG) and magnetic shielding properties at the metal nuclear site for $K[BPh_4]$ and $Na[BPh_4]$. Finally, we perform extensive quantum mechanical calculations for a number of $Na^+-\pi$ and $K^+-\pi$ systems containing common aromatic ligands.

Experimental Section

Sample Preparation. Sodium tetraphenylborate, $Na[BPh_4]$, was obtained from Sigma-Aldrich (Ontario, Canada) and used without further purification. Powder X-ray diffraction measurements suggested that the $Na[BPh_4]$ sample was pure and in the same crystal form as that reported in the literature(see Table 1). Potassium tetraphenylborate, $K[BPh_4]$, was prepared by adding KCl(aq) into an aqueous solution of $Na[BPh_4]$. White fine precipitates were filtered and washed with deionized water. Crystals of $K[BPh_4]$ were grown from acetone/water. The unit cell parameters for $K[BPh_4]$ crystals were determined on a Bruker SMART CCD 1000 X-ray diffractometer with graphite-monochromated Mo Kα radiation ($\lambda = 0.71073$ Å), and were in excellent agreement with the literature values (see Table 1).

TABLE 1: Unit Cell Parameters Determined for $K[BPh_4]$ and $Na[BPh_4]$ by X-ray Diffraction Methods

		unit cell dimension			
compd	diffraction method	*Z*	$a = b$ (Å)	c (Å)	ref
$K[BPh_4]$	single crystal	2	11.221(13)	7.894(6)	17
	single crystal	2	11.211(6)	7.918(7)	this work
	powder	2	11.269(3)	7.913(2)	this work
$Na[BPh_4]$	powder	2	11.45	7.41	18
	powder	2	11.524(8)	7.462(7)	this work

[a] Crystals are tetragonal with space group $I\bar{4}2m$.

Solid-State NMR. Solid-state ^{23}Na and ^{39}K NMR experiments were performed on a Bruker Avance-500 NMR spectrometer (11.75 T) operating at 132.285 and 23.335 MHz for ^{23}Na and ^{39}K nuclei, respectively. The radio frequency (rf) field strength was 90 and 50 kHz at the ^{23}Na and ^{39}K Larmor frequencies, respectively. Static ^{39}K spectra were recorded by using both a Hahn-echo sequence[19] and a Quadrupole Carr−Purcell Meiboom−Gill (QCPMG) sequence.[20] Solid-state ^{23}Na experiments were also performed on a Bruker ASX-200 NMR spectrometer (4.70 T) operating at 52.937 MHz for ^{23}Na. The rf field strength was 77 kHz at the ^{23}Na frequency. Solid-state ^{39}K MAS NMR spectra at 19.6 T (38.718 MHz for ^{39}K nuclei) were obtained at the National High Magnetic Field Laboratory (Tallahassee, Florida), using a Bruker DRX spectrometer and a 4-mm MAS probe. All ^{23}Na and ^{39}K chemical shifts were referenced to NaCl(aq) and KCl(aq), respectively. Spectral simulations were performed with WSOLIDS.[21]

Powder X-ray Diffraction. The powder X-ray diffraction data were collected on a Thermo ARL Scintag ×1 Advanced Diffraction System, using Cu Kα 1 radiation ($\lambda = 1.50562$ Å), with fixed slit widths of 4, 2, 0.5, and 0.2 mm. The data were collected from 5° to 90° 2θ in continuous mode at a rate of 2° per minute with a step increment of 0.02° and preset time of 0.5 s. A high-purity solid-state (liquid nitrogen cooled) germanium detector was used. Data were processed on a Pentium PC, using Thermo ARL Diffraction Management System Software for the Window NT (version 1.39-1B). Background subtraction and smoothing of the raw data were carried out with a boxcar curve fit (filter width of 1.5°) and FFT smoothing (resolution 0.01°). PE Werner's TREOR90 autoindexing program from the Thermo ARL Crystallography (version 1.2) suite was used to determine the unit cell parameters utilizing these Miller indices.

Quantum Mechanical Calculations. All quantum mechanical calculations were performed on a SunFire 6800 symmetric multiprocessor system (24 × 900 MHz processors and 24 GB of memory) with the Gaussian98 suite of programs.[22] Calculations of the ^{23}Na and ^{39}K electric field gradients (EFG) and chemical shielding (σ) parameters for these models were performed at the Hartree−Fock (HF) SCF and density functional theory (DFT) levels with standard basis sets. The principal components of the EFG tensor, q_{ii}, were computed in atomic units (1 au = 9.717365×10^{21} V m^{-2}), with $|q_{zz}| > |q_{yy}| > |q_{xx}|$ and $q_{zz} + q_{yy} + q_{xx} = 0$. The principal magnetic shielding tensor components (σ_{ii}) were computed with $\sigma_{iso} = (\sigma_{11} + \sigma_{22} + \sigma_{33})/3$ and $\sigma_{33} > \sigma_{22} > \sigma_{11}$. In MAS NMR experiments for quadrupolar nuclei, the measurable quantities are the quadrupolar coupling constant (C_Q), the asymmetry parameter (η_Q), and the isotropic chemical shift (δ_{iso}). To make direct comparison between the calculated ^{23}Na and ^{39}K NMR parameters and the experimental results, the following equations were used:

$$C_Q\,[\mathrm{MHz}] = e^2 q_{zz} Q/h = -243.96Q\,[\mathrm{barn}]\cdot q_{zz}\,[\mathrm{au}] \quad (1)$$

$$\eta_Q = (q_{xx} - q_{yy})/q_{zz} \quad (2)$$

$$\delta_{iso} = \sigma_{ref} - \sigma_{iso} \quad (3)$$

where Q is the nuclear quadrupole moment, e is the elementary charge, h is the Planck constant, and σ_{ref} is the magnetic shielding constant for the primary chemical shift reference sample. Standard values of Q were used in this study, $Q(^{23}\mathrm{Na}) = 0.104$ barn and $Q(^{39}\mathrm{K}) = 0.055$ barn (1 barn $= 10^{-28}$ m^2).[23] The primary chemical shift reference is computed for fully hydrated Na^+ and K^+ ions, $[Na(H_2O)_6]^+$ and $[K(H_2O)_6]^+$. The fully optimized MP2/6-311G(d,p) geometries of $[Na(H_2O)_6]^+$ and $[K(H_2O)_6]^+$ were found to have an O_h symmetry with Na−O_w = 2.433 Å and K−O_w = 2.712 Å, respectively. To minimize the systematic basis-set variations, we used these MP2/6-311G(d,p) geometries to calculate σ_{ref} for individual basis sets separately. It should be noted that the computed value of σ_{ref} depends also on the exact geometry used for the hydrated metal ion cluster. For example, $\sigma_{ref}(^{23}\mathrm{Na})$ is 583.70 ppm for $[Na(H_2O)_6]^+$ when the cluster is optimized at the MP2/6-311G(d,p) level. This value is 5.02 ppm smaller than that reported for $[Na(H_2O)_6]^+$ optimized at the HF/6-31G(d) level.[24]

For the first- and second-row elements, we used standard basis sets such as 6-31G(d), 6-311G(d,p), 6-311++G(2d,2p), cc-pVDZ, cc-pVQZ, and Ahlrichs VTZ. For the third-row K atom, we used two different all-electron basis sets. The first one is a medium-size split valence basis set, 6-31G(d), recently reported by Rassolov et al.[25] This basis set has a contraction scheme of (22s, 16p, 1d) → [5s, 4p, 1d]. The second all-electron basis set is a 6-311G type valence triple-ζ basis set reported by Blaudeau et al.[26] This basis set uses a general contraction scheme of (14s, 12p, 3d) → [8s, 7p, 1d]. In addition, various diffuse and polarization functions were also added to the 6-311G type basis set.

Results and Discussion

Powder X-ray Diffraction. In solid-state NMR experiments, one generally uses polycrystalline (or powdered) samples. It is also a common practice among solid-state NMR spectroscopists to rationalize the observed NMR parameters (tensors) in relation to molecular structural features observed in the crystal structure of the compound in question. Because crystal structures are very often determined with X-ray or neutron diffraction experiments on single-crystal samples, it is not always clear whether a particular powder sample used in the NMR experiment should exhibit the same crystal form as that reported in the single-crystal X-ray or neutron diffraction study. One convenient way to check the crystallographic characteristics of the NMR sample is to carry out X-ray powder diffraction measurements. Experimental powder X-ray diffraction spectra for $Na[BPh_4]$ and $K[BPh_4]$ are shown in Figure 2, together with the standard spectra from the ICDD database.[18] On the basis of these X-ray diffraction data, we can conclude that both samples used in our NMR experiments are in the same crystal forms as those used in the previous crystallographic studies. For $K[BPh_4]$, we also performed an independent single-crystal X-ray diffraction experiment, to further confirm that our synthesis had produced the correct compound. Unit cell parameters for $Na[BPh_4]$ and $K[BPh_4]$ are summarized in Table 1. These results firmly established the validity of our interpretation of solid-state NMR data on the basis of crystallographic results.

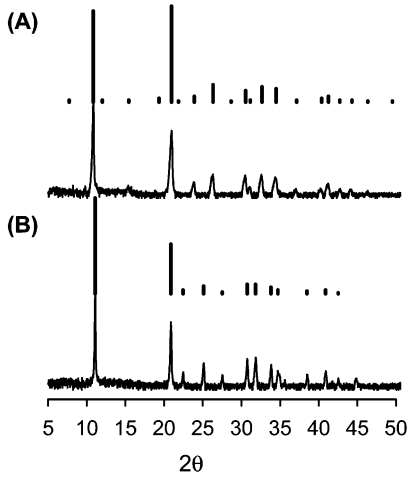

Figure 2. Experimental (trace) and standard (stick) powder X-ray diffraction spectra for (A) $Na[BPh_4]$ and (B) $K[BPh_4]$.

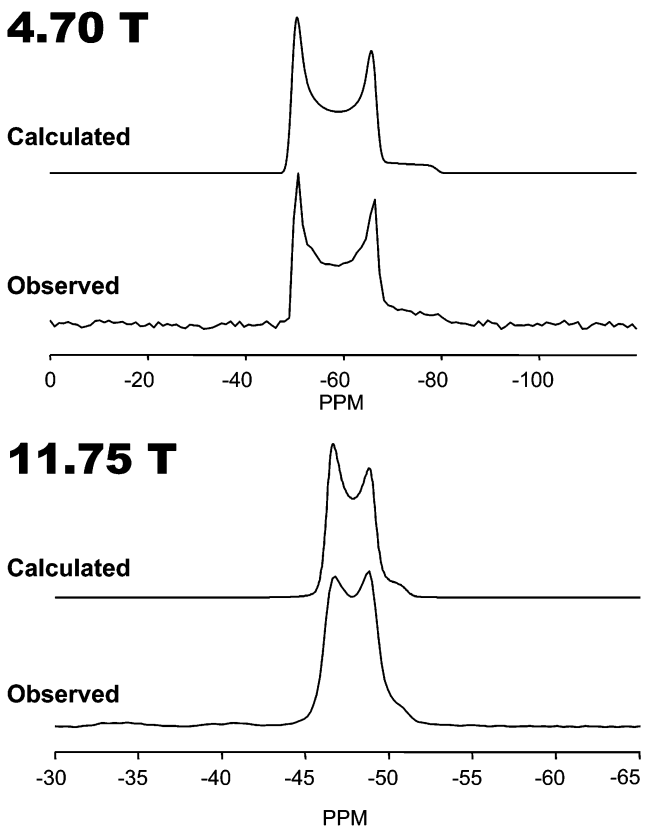

Figure 3. Experimental and calculated ^{23}Na MAS spectra for $Na[BPh_4]$. Experimental parameters are as follows: for 4.70 T, spinning frequency = 15 kHz, 64 transients, recycle delay = 10 s; and for 11.75 T, spinning frequency = 10 kHz, 64 transients, recycle delay = 5 s.

Solid-State NMR. Figure 3 shows the ^{23}Na MAS spectra for $Na[BPh_4]$ at 4.70 and 11.75 T. Each of the spectra exhibits a typical line shape arising from the second-order quadrupole interaction. Simulations of the observed MAS spectra yielded the following ^{23}Na NMR parameters for $Na[BPh_4]$: $|C_Q| = 1.24 \pm 0.05$ MHz, $\eta_Q = 0.0 \pm 0.1$, and $\delta_{iso} = -45.6 \pm 0.5$ ppm. Because the chemical shielding anisotropy (CSA) information is unavailable from MAS spectra, we recorded static spectra for $Na[BPh_4]$ at 4.70 and 11.75 T (see Figure 4). By simultaneously fitting the static spectra recorded at these two fields, we obtained an axially symmetric ^{23}Na chemical shift tensor with a span ($\Omega = \sigma_{33} - \sigma_{11}$) of 14 ± 2 ppm for $Na[BPh_4]$. The unique axis of the ^{23}Na chemical shift tensor is the most

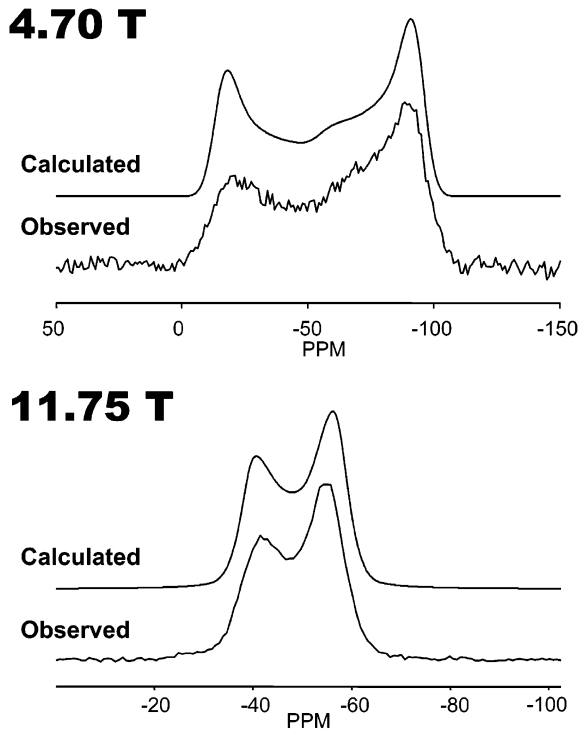

Figure 4. Experimental and calculated ^{23}Na static spectra for Na[BPh_4]. Experimental details are as follows: for 4.70 T, 202 transients, recycle delay = 10 s; and for 11.75 T, 139 transients, recycle delay = 2 s.

shielded. The ^{23}Na NMR tensors found for Na[BPh_4] are quite similar to those reported for sodium metallocenes.[16]

Figure 5 shows the ^{39}K MAS and static spectra for K[BPh_4] obtained at 19.60 and 11.75 T, respectively. Spectral analyses produced the following ^{39}K NMR parameters for K[BPh_4]: $|C_Q| = 1.32 \pm 0.05$ MHz, $\eta_Q = 0.0 \pm 0.1$, and $\delta_{iso} = -92 \pm 1$ ppm. The ^{39}K CSA for K[BPh_4] is too small to be reliably measured. In principle, the ^{39}K CSA for K[BPh_4] should be slightly larger than the ^{23}Na CSA for Na[BPh_4]. However, $\gamma(^{39}K)$ is much smaller than $\gamma(^{23}Na)$, making it difficult to observe small ^{39}K CSA contributions. At 11.75 T, a span of 20 ppm for ^{39}K CSA would contribute only 360 Hz to the total line width of approximately 8 kHz observed for K[BPh_4]. For this reason, it is not possible to accurately determine the ^{39}K CSA for K[BPh_4]. Because of the low ^{39}K NMR frequency, it is generally difficult to obtain high-quality ^{39}K NMR spectra. Larsen et al.[20] demonstrated the use of a QCPMG sequence to improve on the overall sensitivity for ^{39}K NMR experiments. The basic idea of QCPMG is to collect as many echoes as possible during a single excitation. This method is particularly beneficial for samples with relatively long transverse relaxation times. Here we decided to test this approach with K[BPh_4]. The results of the ^{39}K QCPMG experiment for K[BPh_4] are shown in Figure 6. For K[BPh_4], we observed a total of 5 echoes, which corresponds to a transverse relaxation time of approximately 5 ms. As shown in Figure 6B, a direct Fourier transformation of the observed echoes results in a powder pattern composed of spikelets. Another way of processing the QCPMG data is to add all whole echoes together and then to perform Fourier transformation. This data processing method generates a conventional static spectrum as shown in Figure 6C, which can be compared directly with the Hahn-echo spectrum shown in Figure 5B. For K[BPh_4], the sensitivity improvement of the QCPMG experiment is not as large as that demonstrated by Larsen et al.[20] It is likely that the very short T_2 observed for K[BPh_4], 5 ms, diminishes the benefit of the QCPMG experiment in this particular case.

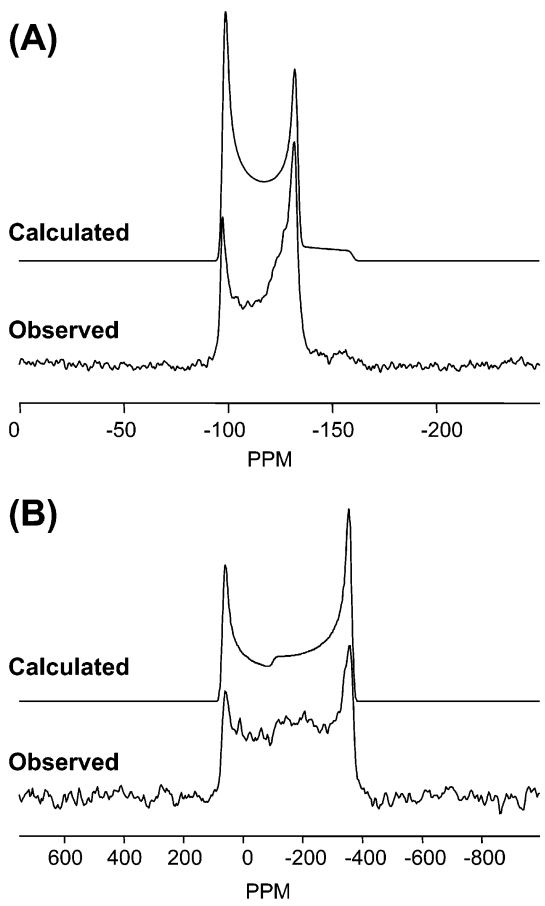

Figure 5. Experimental and calculated ^{39}K NMR spectra for K[BPh_4]. (A) The ^{39}K MAS spectrum was obtained at 19.6 T. Experimental parameters are the following: spinning frequency = 10 kHz, recycle delay = 1 s, 5624 transients. (B) The static ^{39}K spectrum was obtained at 11.75 T, using a Hahn echo sequence. Experimental parameters are the following: recycle delay = 2 s, 83149 transients, total experimental time = 46 h.

Calculations for Na[BPh_4] and K[BPh_4]. To supplement our experimental solid-state NMR data, we performed quantum mechanical calculations of EFG and chemical shielding tensors at the metal site for both Na[BPh_4] and K[BPh_4]. The molecular cluster used in the calculations is depicted in Figure 1C. This molecular cluster has a net charge of −1. We have also tried to use a cluster model containing two more cations along the *c*-axis. The results were essentially the same as those with the cluster model shown in Figure 1C. For K[BPh_4], the crystal structure was used directly in the calculation without geometry optimization.[17] For Na[BPh_4], only unit cell dimensions are known from powder X-ray diffraction studies.[18] Attempts to obtain single crystals for Na[BPh_4] in this laboratory were unsuccessful. Therefore, we decided to construct a cluster model using a combination of powder diffraction data and geometry optimization. In particular, because the Na and B atoms appear at special positions along the *c*-axis of the crystal lattice, the distance between these two atoms is equal to *c*/2 (3.731 Å), which is determined from our powder diffraction experiments (see Table 1). Using this Na−B distance as a constraint, we then fully optimized the cluster structure at the HF/6-31G(d) level. The optimized cluster structure has C_{2v} symmetry. Some structural details for cluster models for Na[BPh_4] and for K[BPh_4] are given in Table 2. Overall, the molecular cluster for Na[BPh_4] is very similar to that for K[BPh_4], except that the distance

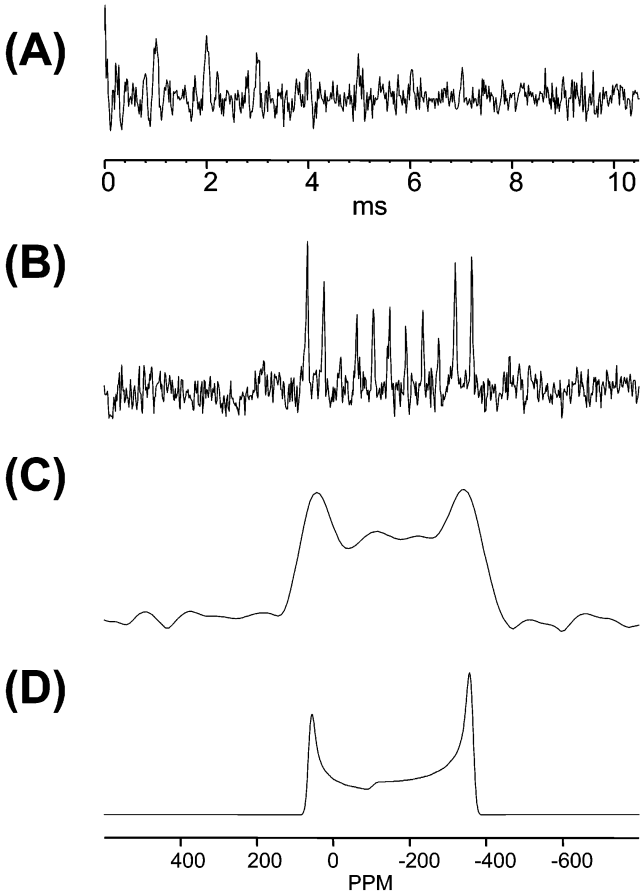

Figure 6. (A) Multiple echos observed in the ^{39}K QCPMG experiment for K[BPh_4] at 11.75 T. The experimental parameters are as follows: A delay of 50 μs after each pulse was used to minimize the effects of acoustic ringing and pulse breakthrough. The acquisition period for each echo was set to 1000 μs, which gives a separation of 1000 Hz between spikelets. Other experimental parameters are the following: dwell time = 10 μs, recycle delay = 2 s, 39325 transients, total experimental time = 22 h. (B) The spikelet QCPMG spectrum produced by direct Fourier transformation of the multiple echos. (C) The static spectrum produced by summing up five QCPMG echos. (D) Calculated static spectrum.

between the Na^+ ion and the center of the phenyl ring is slightly shorter than the corresponding distance in K[BPh_4]. This is in agreement with the expectation that a Na^+ ion interacts with a π system more strongly than does a K^+ ion. This discrepancy between Na^+ and K^+ is also reflected in the unit cell dimensions for the two compounds, c = 7.462 Å for Na[BPh_4] and c = 7.918 Å for K[BPh_4]. The computed ^{23}Na and ^{39}K NMR tensors for Na[BPh_4] and K[BPh_4] are summarized in Table 3. In general, the computed NMR tensors are in reasonable agreement with the experimental values, provided that the basis set used for the metal atom is at a triple-ζ level. For ^{23}Na NMR parameters, it appears that HF/6-31G(d) calculations can also yield reliable results. The accuracy of the computed ^{23}Na NMR parameters for Na[BPh_4] is comparable to that reported in our earlier studies.[28,29] Calculations of ^{23}Na NMR parameters at similar levels of theory have also been reported by Tossell[30] for Na^+ complexes with crown ethers and by Willans and Schurko[16] for sodium metallocenes. For ^{39}K NMR parameters, very little computational data are available in the literature. The calculated results for K[BPh_4] are quite encouraging. As solid-state ^{39}K NMR is becoming feasible,[31] it would be useful to systematically examine the accuracy of the current computation methods in determining ^{39}K NMR properties.

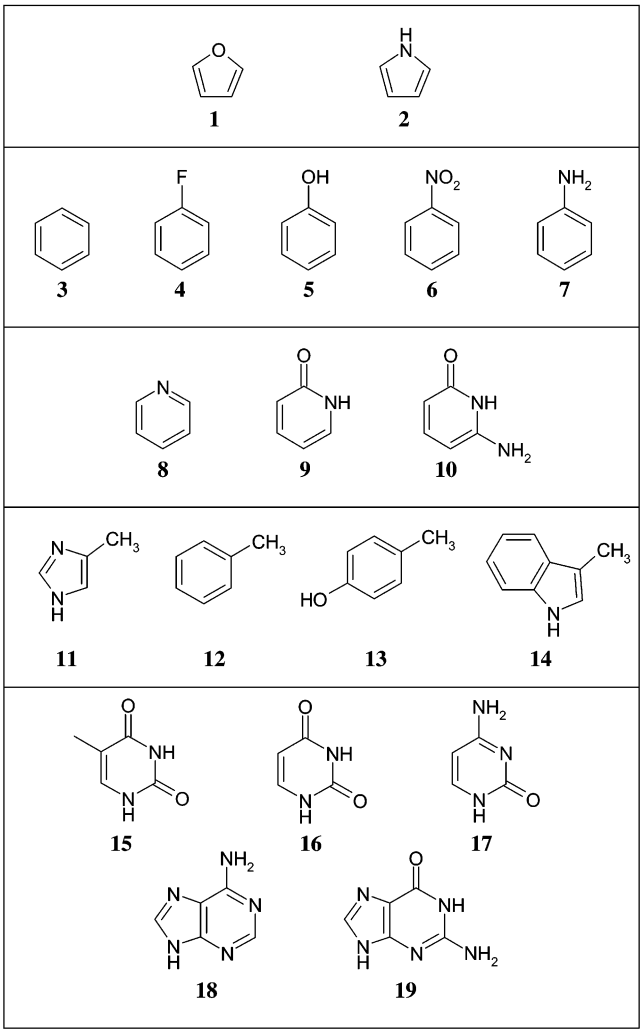

Figure 7. Aromatic molecules used in the quantum mechanical calculations.

Calculations for Model Cation−π Systems. To date there has been very little experimental NMR data for Na^+−π and K^+−π complexes. To establish the general trend in these systems, we employ a computational approach to examine ^{23}Na and ^{39}K NMR parameters for a series of cation−π complexes containing Na^+ and K^+ ions and common aromatic molecules. Figure 7 shows the aromatic compounds used in this study. All molecular geometries used in the computations were optimized at the MP2/6-311G(d,p) level. Optimizations were also performed at HF and B3LYP levels and the computed NMR parameters (data not shown) are similar to those computed with the MP2 structure. The distances between the Na^+ ion and the centroid position of the aromatic plane are found to be in a range between 2.3 and 2.6 Å. The computed ^{23}Na and ^{39}K NMR results for these model complexes are given in Tables 4 and 5, respectively. The values of C_Q(^{23}Na) and C_Q(^{39}K) are in line with those of most of Na^+ and K^+ compounds. One common feature of the computed NMR parameters shown in Tables 4 and 5 is that the metal nucleus is highly shielded in cation−π systems compared with the situations found in most Na^+ and K^+ complexes where the cation is generally coordinated to oxygen and nitrogen ligands. For example, the chemical shifts for the Na−π complexes lie in a narrow range between −33 and −46 ppm. These values are well outside the chemical shift range for most Na compounds, from 20 to −20 ppm. It is also interesting to note that the ^{23}Na chemical shifts for these model

TABLE 2: Selected Distances (Å) and Bond Angles (deg) for Cluster Models of $Na[BPh_4]$ and $K[BPh_4]$

$Na[BPh_4]$[a]				$K[BPh_4]$[b]			
bond		angle		bond		angle	
Na−C(1)	3.017	B−Na−B′	180.0	K−C(1)	3.191	B−K−B′	180.0
Na−C(2)	3.147	C(1)−B−C(1′)	104.8	K−C(2)	3.238	C(1)−B−C(1)	102.8
Na−C(3)	3.472	C(5)−B−C(5′)	103.7	K−C(3)	3.343	C(1)−B−C(1′)	112.9
Na−C(4)	3.640	C(1)−B−C(5)	112.2	K−C(4)	3.403		
		C(1′)−B−C(5′)	112.2				
Na−B	3.731			K−B	3.947		
B−B′	7.462			B−B′	7.894		
B−C(1)	1.672			B−C(1)	1.643		
B−C(5)	1.668						

[a] Fully optimized at the HF/6-31G(d) level. See text for details. [b] From ref 17.

TABLE 3: Experimental and Calculated NMR Parameters for Sodium and Potassium Tetraphenylborates

	method/basis set	σ_{iso} (ppm)	σ_{ref}[a] (ppm)	δ_{iso}[b] (ppm)	Ω[c] (ppm)	C_Q (MHz)
$Na[BPh_4]$	HF/6-31G(d)	625.2	583.7	−41.6	8.9	−1.31
	HF/6-311G(d,p)	622.9	584.9	−38.0	8.8	−1.31
	HF/6-31G(d)/6-311G(d,p)	622.9	583.9	−39.0	9.2	−1.34
	HF/6-31G(d)/6-311++G(2d,2p)	623.0	584.1	−38.9	8.9	−1.32
	HF/6-31G(d)/cc-pVDZ	628.2	588.7	−39.5	8.0	−1.08
	HF/6-31G(d)/Ahlrichs VTZ	621.4	584.7	−36.8	10.5	−1.35
	HF/6-31G(d)/cc-pVQZ	621.6	587.6	−34.0	8.1	−1.24
	B3LYP/6-31G(d)	621.0	563.8	−57.2	9.1	−0.82
	B3LYP/6-311G(d,p)	617.3	571.8	−45.6	8.3	−1.24
	exptl		576.6[d]	−45.6 ± 0.5	14 ± 2	−1.24 ± 0.05[e]
$K[BPh_4]$	HF/6-31G(d)	1349.0	1259.1	−89.8	16.0	−0.69
	HF/6-311G(d,p)	1344.5	1238.4	−106.2	23.4	−1.47
	HF/6-31G(d)/6-311G(d,p)	1346.2	1238.2	−108.0	25.4	−1.41
	HF/6-31G(d)/6-311++G(2d,2p)	1346.7	1237.7	−109.0	25.1	−1.42
	B3LYP/6-31G(d)	1332.2	1242.7	−89.5	13.9	−0.22
	B3LYP/6-311G(d,p)	1320.7	1212.1	−108.6	22.4	−1.27
	B3LYP/6-31G(d)/6-311G(d,p)	1323.0	1211.5	−111.5	25.0	−1.20
	exptl		1271[d]	−92 ± 1		−1.32 ± 0.05[e]

[a] Calculated for $[M(H_2O)_6]^+$ (M = Na and K) fully optimized at the MP2/6-311G(d,p) level. [b] $\delta_{iso} = \sigma_{ref} - \sigma_{iso}$. [c] $\Omega = \sigma_{33} - \sigma_{11}$. [d] From ref 27. [e] The sign of C_Q was assumed on the basis of quantum mechanical calculations.

TABLE 4: Calculated ^{23}Na NMR Parameters for $Na^+-\pi$ Complexes[a,b]

ligand	Na−X distance[c] (Å)	Na−centroid (Å)	δ_{iso} (ppm)	W (ppm)	C_Q (MHz)	η_Q
five-member ring						
1, furan	2.750−2.845	2.533	−40.268	17.183	−1.435	0.756
2, pyrrole	2.640−2.918	2.492	−37.188	24.397	−2.004	0.660
six-member ring						
3, benzene	2.803	2.432	−40.757	18.543	−1.080	0.000
4, fluorobenzene	2.772−2.874	2.511	−41.106	16.714	−1.097	0.037
5, phenol	2.755−2.878	2.378	−40.117	17.559	−1.140	0.088
6, nitrobenzene	2.849−2.866	2.493	−42.723	14.053	−1.078	0.120
7, aniline	2.771−2.826	2.389	−39.934	17.810	−1.124	0.016
8, pyridine	2.744−2.926	2.411	−41.421	16.127	−1.144	0.090
9, $C_5H_4(O)NH$	2.798−2.922	2.425	−36.592	13.919	−1.239	0.425
10, $C_5H_3(O)NHNH_2$	2.735−2.951	2.346	−33.586	11.933	−1.533	0.603
20, $(benzene)_2$	2.800	2.421	−45.479	31.429	−2.185	0.000
aromatic amino acid						
11, histidine	2.833−2.966	2.651	−46.030	12.164	−1.255	0.324
12, phenylalanine	2.774−2.821	2.411	−40.074	19.305	−1.150	0.011
13, tyrosine	2.750−2.838	2.412	−39.859	18.450	−1.183	0.051
14, tryptophan (5 ring)	2.673−2.747	2.434	−40.878	14.396	−1.713	0.505
14, tryptophan (6 ring)	2.700−2.824	2.328	−39.403	24.900	−1.253	0.056
nucleic acid base						
15, thymine	2.925−3.001	2.638	−37.472	7.746	−1.021	0.198
16, uracil	2.972−3.054	2.693	−37.405	7.062	−0.888	0.214
17, cytosine	2.779−2.865	2.435	−36.107	9.720	−1.329	0.663
18, adenine (5 ring)	2.750−2.818	2.516	−43.414	6.819	−1.151	0.390
18, adenine (6 ring)	2.741−2.879	2.449	−42.164	14.590	−1.227	0.340
19, guanine (5 ring)	2.706−2.779	2.473	−44.372	8.657	−1.252	0.460
19, guanine (6 ring)	2.764−2.901	2.475	−39.475	8.154	−1.192	0.193

[a] All structures were optimized at the MP2/6-311G(d,p) level. [b] Both magnetic shielding and EFG calculations were performed at the HF/6-31G(d) level. [c] X refers to C_{Ar}, N_{Ar}, or O_{Ar} atoms.

(gas-phase) $Na^+-\pi$ complexes are quite close to the value for a free Na^+ ion, −39 ppm.[27] This suggests that the weak $Na^+-\pi$ interaction does not cause large perturbations to the electronic structure of the Na^+ ion. Similar trends are also observed for the ^{39}K chemical shifts listed in Table 5.

To further study the ^{23}Na and ^{39}K NMR parameters in cation$-\pi$ systems, we performed a series of computations for Na^+−benzene and K^+−benzene complexes as a function of cation$-\pi$ separation. The calculated results are summarized in Table 6. In general, ^{23}Na and ^{39}K NMR parameters are quite

TABLE 5: Calculated ^{39}K NMR Parameters for $K^+-\pi$ Complexes[a,b]

ligand	K−X distance[c] (Å)	K−centroid (Å)	δ_{iso} (ppm)	W (ppm)	C_Q (MHz)	η_Q
five-member ring						
1, furan	2.962−3.213	2.837	−70.485	38.980	−0.745	0.799
2, pyrrole	2.995−3.145	2.828	−67.614	33.836	−1.214	0.603
six-member ring						
3, benzene	3.201	2.882	−71.715	4.995	−0.742	0.000
4, fluorobenzene	3.149−3.187	2.865	−70.776	7.073	−0.821	0.101
5, phenol	3.103−3.162	2.831	−69.409	9.700	−0.893	0.108
6, nitrobenzene	3.171−3.230	2.881	−71.267	6.034	−0.738	0.168
7, aniline	3.055−3.113	2.752	−70.560	9.175	−0.972	0.105
8, pyridine	3.084−3.265	2.844	−69.306	10.719	−0.776	0.119
9, $C_5H_4(O)NH$	3.172−3.210	2.891	−66.580	15.086	−0.705	0.564
10, $C_5H_3(O)NHNH_2$	3.066−3.270	2.861	−61.900	13.792	−1.109	0.507
20, $(benzene)_2$	3.161, 3.153		−84.195	0.160	−1.730	0.000
aromatic amino acid						
11, histidine	2.850−3.581	2.832	−57.687	21.104	−1.366	0.347
12, phenylalanine	3.109−3.145	2.812	−69.688	9.215	−0.913	0.07
13, tyrosine	3.083−3.139	2.797	−69.348	10.712	−0.926	0.184
14, tryptophan (5 ring)	2.975−3.041	2.763	−68.057	15.418	1.180	0.397
14, tryptophan (6 ring)	3.029−3.128	2.783	−68.029	15.372	1.024	0.070
nucleic acid base						
15, thymine	3.240−3.316	2.990	−65.165	7.493	−0.526	0.070
16, uracil	3.291−3.372	3.048	−64.543	6.953	−0.468	0.088
17, cytosine	3.098−3.204	2.793	−64.532	10.346	−0.783	0.562
18, adenine (5 ring)	3.050−3.114	2.845	−70.034	15.567	−0.772	0.306
18, adenine (6 ring)	3.062−3.186	2.804	−69.519	10.165	−0.719	0.340
19, guanine (5 ring)	3.003−3.068	2.794	−72.763	20.579	−0.771	0.306
19, guanine (6 ring)	3.061−3.185	2.802	−67.591	7.064	−0.664	0.089

[a] All structures were optimized at the MP2/6-311G(d,p) level. [b] Both magnetic shielding and EFG calculations were performed at the HF/6-31G(d) level. [c] X refers to C_{Ar}, N_{Ar}, or O_{Ar} atoms.

TABLE 6: Calculated ^{23}Na and ^{39}K NMR Parameters for Cation−Benzene Complexes[a]

system	M−C_{Ar} (Å)	M−centroid (±0.05 Å)	δ_{iso} (ppm)	$\delta_\perp$ (ppm)	$\delta_{\|}$ (ppm)	W (ppm)	C_Q (MHz)
Na^+−benzene	1.997	1.42	59.36	107.020	−35.864	142.884	5.493
	2.460	2.02	−25.146	−9.939	−55.511	45.572	−0.724
	2.803	2.42	−40.757	−34.575	−53.119	18.544	−1.080
	3.150	2.82	−44.732	−42.224	−49.699	7.475	−0.750
	3.697	3.42	−43.576	−42.348	−46.004	4.351	−0.250
free Na^+ ion			−39.542				
K^+−benzene	1.997	1.42	349.916	525.739	−1.117	526.856	3.614
	2.460	2.02	23.500	71.454	−72.266	143.720	−2.737
	3.150	2.82	−70.427	−67.915	−75.331	7.416	−0.830
	3.697	3.42	−73.500	−72.298	−74.131	1.833	−0.227
	4.070	3.82	−71.449	−70.817	−71.785	0.968	−0.129
	4.733	4.52	−68.551	−68.255	−69.123	0.868	−0.078
free K^+ ion			−66.013				

[a] Both magnetic shielding and EFG calculations were performed at the HF/6-31G(d) level.

sensitive to the cation−benzene distance. As shown in Figure 8, the value of C_Q shows an interesting dependence on the cation−benzene separation. When the metal ion is far away from the benzene ring (>3.5 Å), the EFG at the metal nucleus is essentially zero, just as the case for a free ion. As the cation−benzene distance gets shorter, negative values of C_Q are observed. When the cation−benzene separation reaches a critical distance (approximately 1.9 and 1.8 Å for Na^+−benzene and for K^+−benzene, respectively), the EFG at the metal nucleus vanishes. For distances below this critical distance, C_Q becomes positive and increases drastically with a decrease of the cation−benzene separation. This observation immediately suggests that, when Na^+ and benzene are sufficiently close, the spherically distributed orbitals of Na^+ are "polarized" by the benzene molecule to induce an opposite EFG that partially cancels the EFG generated by the benzene molecule itself. However, one should exercise caution in interpreting these data, because the very short cation−benzene distances may not be realistic.

The magnetic shielding at the metal nucleus also shows an interesting dependence on the cation−benzene separation. More specifically, the metal nucleus becomes significantly less shielded (with positive chemical shifts) when the cation is moved close to the benzene ring. This clearly suggests that the diamagnetic ring current does not play any significant role in this case, because it would cause an increase in magnetic shielding at the metal nucleus. Further examination of the chemical shift tensor components reveals that only the magnetic shielding along the directions perpendicular to the C_6 axis ($\sigma_\perp$) changes as the cation approaches the benzene, whereas the magnetic shielding along the C_6 axis ($\sigma_{\|}$) remains at a value very similar to that for a free ion. For a free ion, the origin of magnetic shielding is purely diamagnetic according to the Ramsey formalism. For cation−benzene complexes, the calculations show that the paramagnetic shielding contribution becomes important as the cation is moved toward the benzene. This is similar to the case of decamethylaluminocenium cation reported by Schurko et al.[32] A detailed analysis of the paramagnetic contributions from individual molecular orbitals for $Na[BPh_4]$ and $K[BPh_4]$ is beyond the scope of this paper.

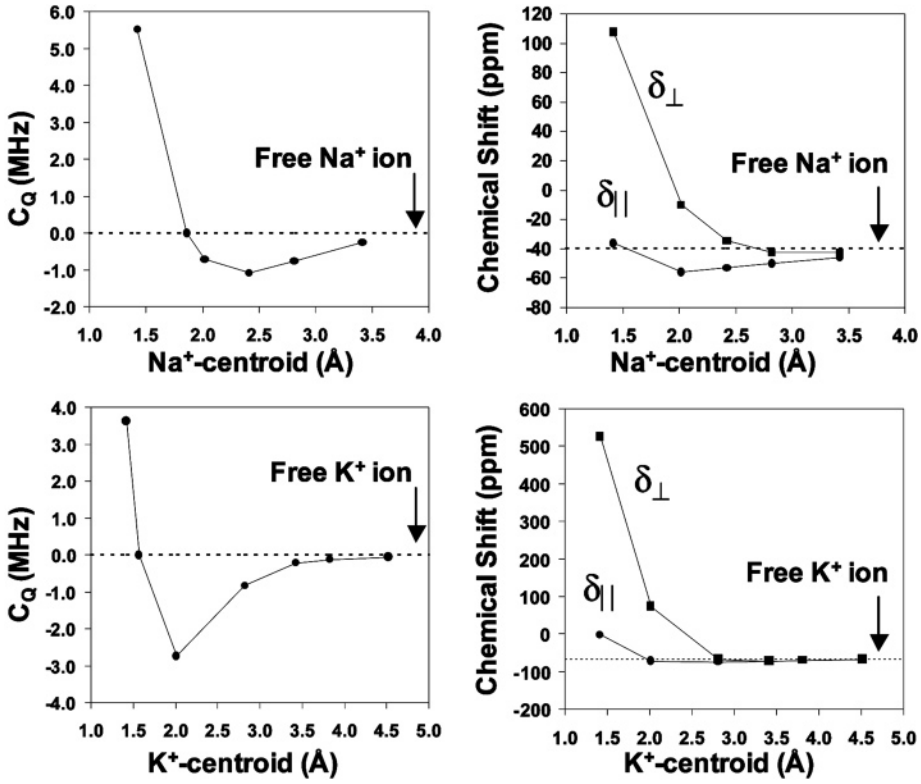

Figure 8. Computed NMR parameters for Na^+− and K^+−benzene complexes as a function of cation−centroid distance. The chemical shift tensor components, $\delta_\perp$ and $\delta_{||}$, correspond to directions perpendicular and parallel to the C_6 axis of the complex, respectively.

Conclusions

We have obtained solid-state ^{23}Na and ^{39}K NMR spectra for $Na[BPh_4]$ and $K[BPh_4]$ at 4.70, 11.75, and 19.60 T. The ^{23}Na and ^{39}K chemical shifts found for $Na[BPh_4]$ and $K[BPh_4]$ are among the most shielded values compared with other sodium and potassium compounds. Extensive quantum mechanical calculations have confirmed that the highly shielded (with very negative chemical shifts) environment at the metal site is a characteristic feature for cations in cation−π systems. This NMR signature may be useful in interpreting NMR signals from cations that are involved in cation−π interactions in proteins and nucleic acids.

Acknowledgment. This research was supported by the Natural Sciences and Engineering Research Council (NSERC) of Canada. All quantum mechanical calculations were performed at the High Performance Computing Virtual Laboratory (HPCVL) at Queen's University. G.W. thanks Queen's University for a Chancellor's Research Award and the Province of Ontario for a Premier's Research Excellence Award. A.W. thanks the Province of Ontario for an Ontario Graduate Scholarship. We are also grateful to anonymous reviewers for helpful suggestions.

References and Notes

(1) Dougherty, D. A. *Science* **1996**, *271*, 163−168.
(2) Ma, J. C.; Dougherty, D. A. *Chem. Rev.* **1997**, *97*, 1303−1324.
(3) Gokel, G. W.; Barbour, L. J.; De Wall, S. L.; Meadows, E. S. *Coord. Chem. Rev.* **2001**, *222*, 127−154.
(4) Gallivan, J. P.; Dougherty, D. A. *Proc. Natl. Acad. Sci. U.S.A.* **1999**, *96*, 9459−9464.
(5) Wintjens, R.; Lievin, J.; Rooman, M.; Buisine, E. *J. Mol. Biol.* **2000**, *302*, 395−410.
(6) Nayal, M.; Di Cera, E. *J. Mol. Biol.* **1996**, *256*, 228−234.
(7) Tereshko, V.; Wilds, C. J.; Minasov, G.; Prakash, T. P.; Maier, M. A.; Howard, A.; Wawrzak, Z.; Manoharan, M.; Egli, M. *Nucleic Acids Res.* **2001**, *29*, 1208−1215.
(8) Wouters, J. *Protein Sci.* **1998**, *7*, 2472−2475.
(9) Wouters, J.; Maes, D. *Acta Crystallogr. Sect. D* **2000**, *56*, 1201−1203.
(10) De Wall, S. L.; Meadows, E. S.; Barbour, L. J.; Gokel, G. W. *Proc. Natl. Acad. Sci. U.S.A.* **2000**, *97*, 6271−6276.
(11) Sarkhel, S.; Rich, A.; Egli, M. *J. Am. Chem. Soc.* **2003**, *125*, 8998−8999.
(12) Matthews, S. E.; Rees, N. H.; Felix, V.; Drew, M. G. B.; Beer, P. D. *Inorg. Chem.* **2003**, *42*, 729−734.
(13) Pietrass, T.; Burkert, P. K. *Inorg. Chim. Acta* **1993**, *207*, 253−254.
(14) Johnels, D.; Boman, A.; Edlund, U. *Magn. Reson. Chem.* **1998**, *36*, S151−S156.
(15) Jost, S.; Günther, H. *Magn. Reson. Chem.* **2003**, *41*, 373−378.
(16) Willans, M. J.; Schurko, R. W. *J. Phys. Chem. B* **2003**, *107*, 5144−5161.
(17) Horffmann, K.; Weiss, E. *J. Organomet. Chem.* **1974**, *67*, 221−228.
(18) The International Centre for Diffraction Data (ICDD) Powder Diffraction File PDF-2 Database Sets 1−46.
(19) Kunwar, A. C.; Turner, G. L.; Oldfield, E. *J. Magn. Reson.* **1986**, *69*, 124−127.
(20) (a) Larsen, F. H.; Jakobsen, H. J.; Ellis, P. D.; Nielsen, N. C. *J. Phys. Chem. A* **1997**, *101*, 8597−8606. (b) Larsen, F. H.; Skibsted, J.; Jakobsen, H. J.; Nielsen, N. C. *J. Am. Chem. Soc.* **2000**, *122*, 7080−7086.
(21) For information about WSOLIDS, please contact Dr. Klaus Eichele, http://casgm3.anorg.chemie.uni-tuebingen.de/klaus/soft/index.html.
(22) Frisch, M. J.; Trucks, G. W.; Schlegel, H. B.; Scuseria, G. E.; Robb, M. A.; Cheeseman, J. R.; Zakrzewski, V. G.; Montgomery, J. A.; Stratmann, R. E.; Burant, J. C.; Dapprich, S.; Millam, J. M.; Daniels, A. D.; Kudin, K. N.; Strain, M. C.; Farkas, O.; Tomasi, J.; Barone, V.; Cossi, M.; Cammi, R.; Mennucci, B.; Pomelli, C.; Adamo, C.; Clifford, S.; Ochterski, J.; Petersson, G. A.; Ayala, P. Y.; Cui, Q.; Morokuma, K.; Malick, D. K.; Rabuck, A. D.; Raghavachari, K.; Foresman, J. B.; Cioslowski, J.; Ortiz, J. V.; Stefanov, B. B.; Liu, G.; Liashenko, A.; Piskorz, P.; Komaromi, I.; Gomperts, R.; Martin, R. L.; Fox, D. J.; Keith, T.; Al-Laham, M. A.; Peng, C. Y.; Nanayakkara, A.; Gonzalez, C.; Challacombe, M.; Gill, P. M. W.; Johnson, B.; Chen, W.; Wong, M. W.; Andres, J. L.; Head-Gordon, M.; Replogle, E. S.; Pople, J. A. *Gaussian 98*, Revision A.6; Gaussian, Inc.: Pittsburgh, PA, 1998.
(23) Akitt, J. W. In *Multinuclear NMR*; Mason, J., Ed.; Plenum Press: New York, 1987; pp 189−220.
(24) Tossell, J. A. *Phys. Chem. Miner.* **1999**, *27*, 70−80.
(25) Rassolov, V. A.; Pople, J. A.; Ratner, M. A.; Windus, T. L. *J. Chem. Phys.* **1998**, *109*, 1223−1230.

(26) Blaudeau, J.-P.; McGrath, M. P.; Curtiss, L. A.; Radom, L. *J. Chem. Phys*. **1997**, *107*, 5016−5021.
(27) Jameson, C. J.; Mason, J. In *Multinuclear NMR*; Mason, J., Ed.; Plenum Press: New York, 1987; Chapter 3.
(28) Wong, A.; Wu, G. *Can. J. Anal. Sci. Spectrosc*. **2001**, *46*, 188−197.
(29) Wong, A.; Wu, G. *J. Phys. Chem. A* **2003**, *107*, 579−586.
(30) Tossell, J. A. *J. Phys. Chem. B* **2001**, *105*, 11060−11066.
(31) Wu, G.; Wong, A.; Gan, Z.; Davis, J. T. *J. Am. Chem. Soc*. **2003**, *125*, 7182−7183.
(32) Schurko, R. W.; Hung, I.; Macdonald, C. L. B.; Cowley, A. H. *J Am. Chem. Soc*. **2002**, *124*, 13204−13214.